

# Modal Dynamics of NREL 5MW Wind Turbine During Normal and Parked Conditions

S. A. Sina<sup>1\*</sup> and B. Balanian<sup>2</sup>

1. Faculty of Mechanical Engineering, Shahrood University of Technology, Shahrood, Iran.  
2. Aerospace Engineering Department, Sharif University of Technology, Tehran, Iran

Received Date 05 June 2022; Revised Date 16 August 2022; Accepted Date 20 August 2022  
Corresponding author: a.sina@shahroodut.ac.ir (S. A. Sina)

## Abstract

The multi-Megawatt wind turbines have long, slender, and heavy blades that can undergo extremely wind loadings. A good understanding of the modal dynamics of these large machines is of great priority. In this work, the modal dynamics of the NREL 5 MW wind turbine is investigated. For this aim, the FAST software is implemented. The vibration characteristics of blades, tower, and whole wind turbine machine are extracted. In order to examine the effects of wind velocity, two operating conditions of machine are considered, namely the normal operating condition at rated wind velocity and rated rotor speed, and the other, the parked condition with fixed rotor at the wind velocity equal to rated wind velocity. The blade root bending moments (both in plane and out of plane) and tower bending moments (both longitudinal and lateral) are extracted. The frequency spectrum of the results is utilized as a tool to study the effects of each vibration mode on the wind turbine dynamics in each aforementioned operating condition. It is shown that tower vibration during normal operation is highly influenced from the blade edge-wise bending mode. On the other hand, during the parked condition, the effects of flap-wise bending modes become more dominant. The results are expected to offer better predictions of the vibrational behavior of large wind turbines.

**Keywords:** Wind turbine, Structural dynamics, Parked condition, Vibration, Campbell diagram.

## 1. Introduction

Renewable energies have numerous socio-economic benefits including lower carbon emissions, lower air pollution, growing number of jobs, and improved reliability in conjunction with rapidly falling technology costs. One of the fastest-growing renewable energy technologies is wind power 0-0 as the installed capacity of wind power increased by a factor of 75 in the past two decades, and doubled between 2014 and 2020 and the global installed capacity in 2020 reaches 744 GW 0. As the technology matured, different simulation tools have been developed for wind turbines in order to attain machines with maximum energy production and lowest cost. Generally, wind power system design has three important purposes: minimize the structural loads to extend turbines lifetime, maximize power, and more grid integrity.

Wind energy costs have had significant reductions during the last decades, and consequently, have huge increment in size. This increment leads to a larger swept area, and consequently, more wind energy capture and reduced energy costs. As

turbine blades become larger, they also get more flexible. More flexibility makes several challenges in the wind turbine design.

Early design tools were based on simple aerodynamic tools such as blade element momentum theory to calculate blade loading. Recent development in wind turbine design leads to similar development in design tools that can provide accurate simulation of the wind turbine loading and performance. FAST is the National Renewable Energy Laboratory (NREL) of the USA main simulation tool for simulating the operation of complete wind turbine. FAST considers aerodynamics, control and electrical system dynamics, and structural dynamics models to enable coupled non-linear aero-hydro-servo-elastic simulation in the time domain. The FAST software performs the simulation of a range of wind turbine configurations: two- or three-blade horizontal axis rotor, pitch or stall regulation, rigid or teetering hub, upwind or downwind rotor, and lattice or tubular tower. FAST is based on advanced engineering models—derived from

fundamental laws but with appropriate simplifications and assumptions, and supplemented where applicable with computational solutions and test data [1].

Wind turbine rotors in certain conditions such as in extreme wind speeds or during maintenance, can be stopped: in a fully locked state or in an idling state with a very slow rotational speed. In such conditions, the blades are pitched  $90^\circ$  to break the rotor aerodynamically. This operating condition is entitled as parked configuration. Modern Mega Watt (MW)-sized horizontal axis wind turbines have highly flexible blades made from composite materials. The parked configuration is susceptible to dangerous vibration that can arise from the coupled effects between the unsteady flow loading and the elastic blades. One of the plausible causes for this so-called standstill vibration is related to the phenomenon vortex-induced vibration that may occur when the incoming flow causes angles of attack in the vicinity of  $\pm 90^\circ$ . In this angle of attack range, periodic vortex shedding is common, and its interaction with the structural modes of the blades can potentially lead to large amplitudes of vibration.

Several numerical studies have addressed the topic of wind turbine blade standstill vibrations by the use of fluid-structure interaction. Heinz *et al.* [2] have studied the 86-m-long blade of the DTU 10 MW reference wind turbine [3], predicting vibrations for several inflow configurations impinging the surface from the pressure side. The initial simulations assumed the blade to point upward. The wind speed magnitude was varied along the span, consistent with the blade tapering, in order to target a constant strouhal number for each one of the sections. This unrealistic inflow led to large edge-wise vibrations for values of strouhal number in the vicinity of 0.15, which is a typical value for airfoils at the studied Reynolds number [4], and the wake showed spanwise correlated shedding. This indicated a potential relation between the tackled instability and the widely studied vortex induced vibration phenomenon for two-dimensional geometries in transverse motion. Similar observations were made when replicating the study around the uniform inflow on the 100-m-long blade of the AVATAR reference wind turbine [5]. Horcas *et al.* [6] have studied standstill vibrations of wind turbines. Five different variations of a reference turbine blade model developed in the framework of the International Energy Agency (IEA) wind technology collaboration program, referred to as IEA 10MW [7], were studied. The authors related

the observed inclination angle bounds of instability to limits in the effective velocity characterizing the problem. This was done through the independence principle [8] that states that for an inclined inflow the emergence of vortex induced vibration is steered by the sectional component of the velocity. This confined manifestation of the vibrations in terms of effective wind speed, which is a signature of vortex induced vibration, was also found in the work of Horcas *et al.* [6] based on the AVATAR blade. In general, all the previous works pointed toward wind turbine blades experiencing an instability that can be categorized as vortex induced vibration. Such vibrations can influence the structural integrity of the wind turbine. Hence, it is so important to understand the underlying interacting vibration modes in this phenomenon, which is the main motivation of the present research work.

In order to investigate the modal characteristics of wind turbine at parked condition, it is important to identify the dominant vibration modes in this turbine operating condition. Also variation of modal characteristics in different wind speed and rotor rotational velocity should be outlined. This work aims to investigate the vibration characteristics of wind turbine at parked condition. In this regards, the wind turbine has been simulated using FAST, and the simulation results are investigated. Modal dynamics of wind turbine, variation of vibration characteristics versus wind speed will be addressed in detail. The paper is organized as what follows. The FAST software and some important aeroelastic phenomena of wind turbine in standstill operating condition will be introduced. Then the FAST software and the behind concepts will be addressed. Afterwards, the simulation results will be analyzed in the context of classical structural dynamic concepts, and some important conclusions will be outlined.

## 2. NREL FAST solver

FAST is a fatigue, aerodynamic, structural, and turbulence analysis multi-physics engineering software specialized for wind energy applications. The tool has an aero-hydro-servo-elastic capability for full-scale simulation horizontal axis wind turbines operating in several conditions. FAST allows one to perform load and stability analysis, and obtain performance data. The computer-aided engineering tool is actively developed and maintained by NREL. FAST is open-source available for free. FAST has been validated by measurements and verified, and

hence, widely employed in the industry. FAST 8, the latest version, consists of several modules for modeling physics efficiently. It utilizes low-order models that reduce computational cost. The modules available in the FAST solver are:

- AeroDyn for rotor aerodynamics
- HydroDyn for hydro-dynamics
- ServoDyn for control and electrical system dynamics
- ElastoDyn for structural dynamics, TurbSim for generating turbulent inflow wind.

These modules are coupled into a tool that enables performing aero-hydro-servo-elastic analysis of wind turbines. The inputs and outputs connect several of the modules for specialized applications. For example, TurbSim can generate inflow wind field for use by AeroDyn module, and then AeroDyn solves for the aerodynamic loads applying its BEM solver, and then ElastoDyn to obtain blade deformations, etc.

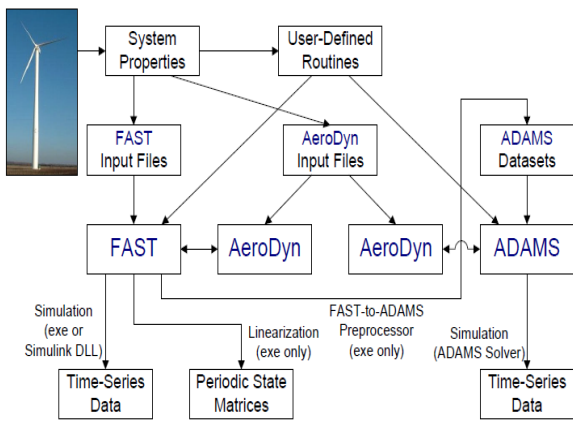


Figure 1. FAST: Modes of operation 0.

The interested readers could find a detail survey on FAST operation and analytical concepts behind it in 0.

### 3. NREL 5MW wind turbine

The description and all values of the NREL 5MW parameters are tabulated in table 1.

The structural properties of blade, nacelle, and tower are tabulated in tables 2 to 4.

The first and second mass moments of inertia in Table 2 are calculated with respect to the blade’s root. A detailed structural and aeroelastic analysis of NREL 5 MW blade is represented in 0.

Table 4 represents the overall properties of the tower. Figure 2 shows a schematic description of the tower.

Table 1. Parameters of NREL 5 MW wind turbine model 0.

| Description               | Value    | Unit              |
|---------------------------|----------|-------------------|
| Number of blades          | 3        | -                 |
| Rotor inertia             | 38759227 | kg.m <sup>2</sup> |
| Generator inertia         | 534      | kg.m <sup>2</sup> |
| Air density               | 1.2256   | kg/m <sup>3</sup> |
| Rotor radius              | 63       | m                 |
| Overhang                  | 5        | m                 |
| Hub height                | 90       | m                 |
| Shaft tilt, Precone       | 5, 2.5   | deg               |
| Rotor mass                | 110000   | kg                |
| Nacelle mass              | 240000   | kg                |
| Tower mass                | 347460   | kg                |
| Gearbox ratio             | 97       | -                 |
| Cut-in speed              | 3        | m/s               |
| Cut-out speed             | 25       | m/s               |
| Rated speed               | 11.4     | m/s               |
| Cut-in rotor speed        | 6.9      | rpm               |
| Rated rotor speed         | 12.1     | rpm               |
| Rated power               | 5296610  | W                 |
| Maximum power coefficient | 0.4771   | -                 |
| Maximum generator torque  | 43093.55 | N.m               |

Table 2. NREL 5MW blade’s structural properties 0.

| Description                                    | Value    | Unit              |
|--|----------|-------------------|
| Length (along pre-coned axis)                  | 61.5     | m                 |
| Second mass moment of inertia                  | 11776047 | kg.m <sup>2</sup> |
| First mass moment of inertia                   | 363231   | kg.m              |
| mass   | 17740    | kg                |
| Center of mass location (along pre-coned axis) | 20.475   | m                 |
| Structural damping ratio                       | 0.477465 | -                 |

Table 3. NREL 5MW nacelle’s structural properties 0.

| Description  | Value   | Unit              |
|--|---------|-------------------|
| Elevation of Yaw Bearing above Ground                      | 87.6    | m                 |
| Vertical distance along Yaw Axis from Yaw Bearing to Shaft | 1.96256 | m                 |
| Distance along shaft from hub center to yaw axis           | 5.0191  | m                 |
| Distance along shaft from hub center to main bearing       | 1.912   | m                 |
| Hub mass   | 56780   | kg                |
| Hub inertia about low-speed shaft                          | 115926  | kg.m <sup>2</sup> |
| Nacelle mass   | 240000  | kg                |
| Nacelle Inertia about yaw axis                             | 2607890 | kg.m <sup>2</sup> |
| Nacelle center of mass location downwind of yaw axis       | 1.9     | m                 |
| Nacelle center of mass location above yaw bearing          | 1.75    | m                 |

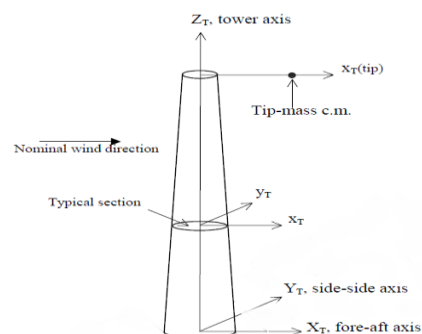


Figure 2. Schematic description of wind turbine tower 0.

**Table 4. NREL 5MW tower’s structural properties 0.**

| Description  | Value              | Unit     |
|--|--------------------|----------|
| Height above ground                                | 87.6               | m        |
| Overall mass                                       | 347460             | kg       |
| Overall mass top of tower                          | 356000             | kg       |
| Center of mass location along tower centerline     | 38.234             | m        |
| $I_{xx}$   | $4.37 \times 10^7$ | $kg.m^2$ |
| $I_{yy}$   | $2.35 \times 10^7$ | $kg.m^2$ |
| $I_{zz}$   | $2.54 \times 10^7$ | $kg.m^2$ |
| Distance between nacelle mass and tower centerline | 1.97               | m        |
| Diameter of bottom section                         | 6                  | m        |
| Thickness at bottom section                        | 0.027              | m        |
| Diameter of top section                            | 3.87               | m        |
| Thickness at top section                           | 0.019              | m        |
| Young modulus                                      | 210                | GPa      |
| Shear modulus                                      | 80.8               | GPa      |
| Effective density                                  | 8500               | $kg/m^3$ |
| Structural damping ratio                           | 1                  | %        |

### 4. Simulation results

#### 4.1. Blade and tower: modal dynamics

First 20 natural frequencies of the blade are depicted in table 5.

**Table 5. First 20 natural frequencies (N.F.s) of NREL 5 MW blade**

| No. | N.F. (Hz) |
|-----|-----------|-----|-----------|-----|-----------|-----|-----------|
| 1   | 0.861     | 6   | 4.641     | 11  | 12.533    | 16  | 18.942    |
| 2   | 1.129     | 7   | 7.618     | 12  | 14.687    | 17  | 23.082    |
| 3   | 2.148     | 8   | 7.996     | 13  | 15.246    | 18  | 25.205    |
| 4   | 4.042     | 9   | 9.260     | 14  | 16.675    | 19  | 26.440    |
| 5   | 4.196     | 10  | 11.226    | 15  | 18.091    | 20  | 27.729    |

Figure 3 shows the natural frequencies of the first and second vibration modes of the blades versus blade.

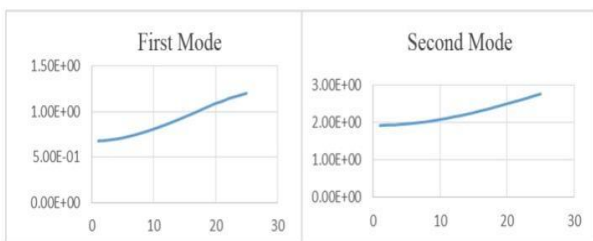


**Figure 3. Variation of first and second mode natural frequencies (Hz) versus blade rotational speed (rpm).**

rotational speed. The depicted results show the stiffening effect of rotational speed on the first 2 vibration modes of the blade. Figure 4 shows the most important degrees of freedom in wind turbine rotor, blade, and tower.

Figures 5 (a), (b) show the Campbell diagram of blade.

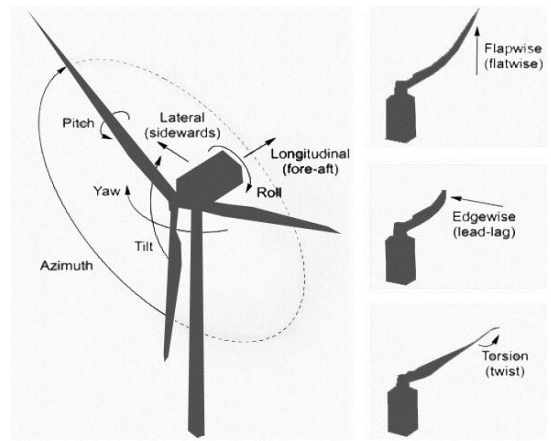
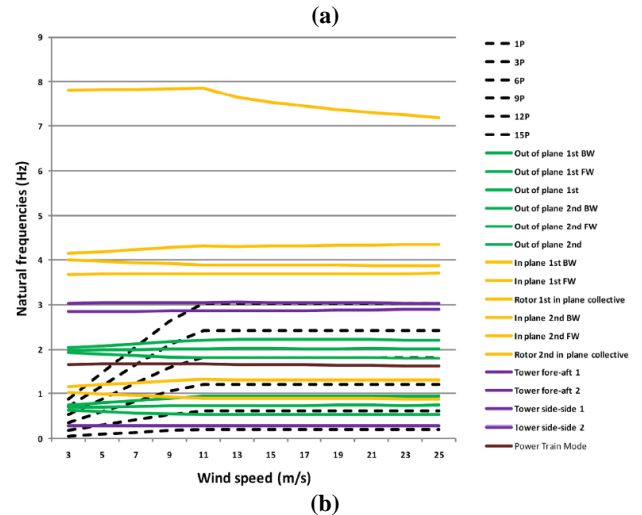
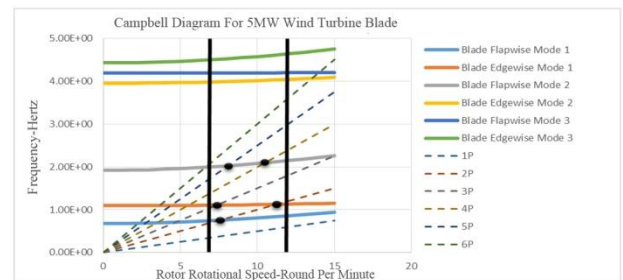


**Figure 4. Wind turbine rotor, blade, and tower degrees of freedom 0.**



**Figures 5. Campbell diagram of NREL 5 MW wind turbine blade, (a): in different rotational speeds, (b): in different wind speeds.**

Variation of different blade’s structural vibration modes in different rotational speed and wind velocities are depicted in figures 5-(a) and 5-(b), respectively. The 6 first vibration modes of blade are bending modes. Two vertical solid lines represent the bands of rated speed. Also intersection of vibration modes with multiples of blade rotational speed is highlighted, and operation of wind turbine at these points should be avoided.

Table 6 represents 20 first natural frequencies of the tower. Dominant deformation of each

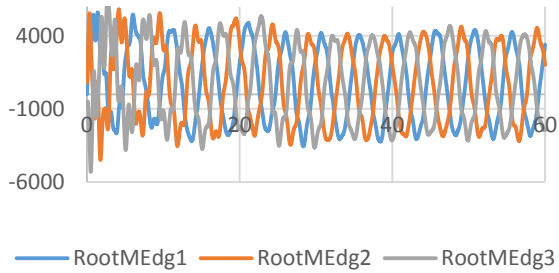
vibration mode is included.

**Table 6. First 20 natural frequencies (N.F.s) of NREL 5 MW tower with/without top mass (W./W.O. T.M.). SS: Side-Side, FA: Fore-Aft, T; Torsion, A: Axial.**

| No. | Mode | W. T.M. | W.O.T.M. | No. | Mode | W. T.M. | W.O.T.M. |
|-----|------|---------|----------|-----|------|---------|----------|
| 1   | SS   | 0.88    | 0.32     | 11  | T    | 35.76   | 21.75    |
| 2   | FA   | 0.88    | 0.32     | 12  | SS   | 35.76   | 21.81    |
| 3   | SS   | 4.36    | 1.52     | 13  | FA   | 35.96   | 23.55    |
| 4   | FA   | 4.36    | 1.88     | 14  | A    | 43.40   | 35.74    |
| 5   | SS   | 11.35   | 2.28     | 15  | T    | 53.28   | 35.78    |
| 6   | FA   | 11.35   | 4.66     | 16  | SS   | 53.28   | 43.40    |
| 7   | T    | 15.09   | 5.08     | 17  | FA   | 58.37   | 46.41    |
| 8   | A    | 16.50   | 11.33    | 18  | T    | 71.36   | 53.34    |
| 9   | SS   | 21.79   | 11.47    | 19  | A    | 74.33   | 53.36    |
| 10  | FA   | 21.79   | 16.50    | 20  | SS   | 74.34   | 69.42    |

### 4.2. Wind turbine normal operation at rated speed

In this section, the NREL 5MW in the onshore configuration is considered. The normal operation of wind turbine at the wind velocity of 11.4 mps and rotor speed of 12.1 rpm is considered.



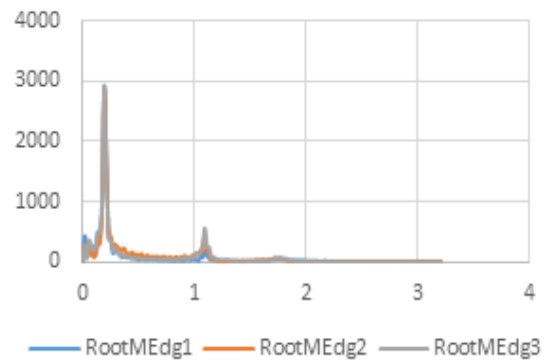
**Figure 6. Root edge-wise bending moment (kN.m) of NREL 5MW blades time history at normal operation, wind velocity of 11.4 mps and rotor speed of 12.1 rpm.**

Figure 6 represents the root edge-wise bending moment of blades. The results show the in-phase motion of two blades and out of phase deformation of third blade in comparison with two other blades. Hence, the dominant edge-wise bending mode of rotor is asymmetric mode, as shown in figure 7.



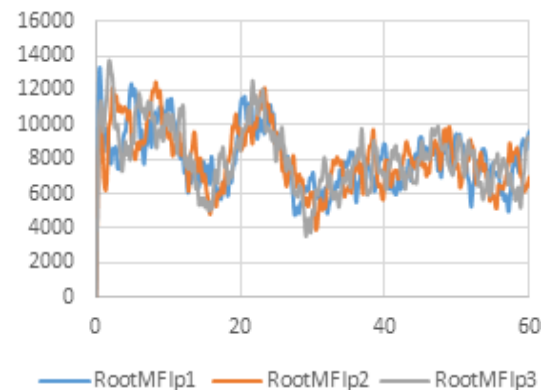
**Figure 7. Schematic description of asymmetric edge-wise bending mode of rotor 0.**

The frequency content of the root edge-wise bending moment is represented in figure 8.



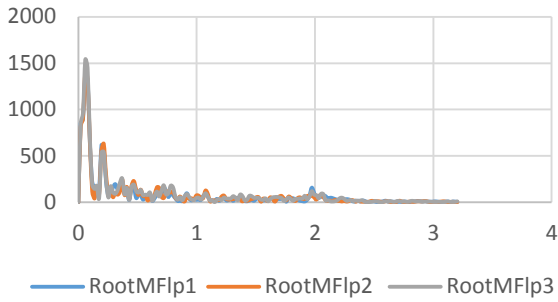
**Figure 8. Frequency (Hz) spectrum of root edge-wise bending moment of NREL 5MW blades at normal operation, wind velocity of 11.4 mps and rotor speed of 12.1 rpm.**

Figure 9 represents the root flap-wise bending moment of blades. The quasi static deformation of blades in flap is shown.



**Figure 9. Root flap-wise bending moment (kN.m) of NREL 5MW blades time history at normal operation, wind velocity of 11.4 mps and rotor speed of 12.1 rpm.**

The frequency content of the root edge-wise bending moment is represented in figure 10. It should be noted that the first peak at 0.2 Hz in both figure 8 and figure 10 correspond to the rotor rotating speed of 12.1 rpm.



**Figure 10.** Frequency (Hz) spectrum of root flap-wise bending moment of NREL 5MW blades at normal operation, wind velocity of 11.4 mps and rotor speed of 12.1 rpm.

For-aft and side-side bending moments of the tower are depicted in figure 11 and figure 12. Also the corresponding frequency spectrums are represented in figure 13 and figure 14.

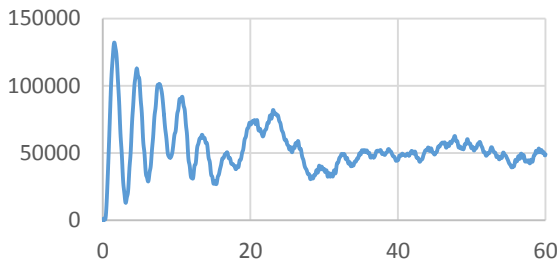


**Figure 11.** For-aft bending moment (kN.m) of NREL 5MW tower time history at normal operation, wind velocity of 11.4 mps and rotor speed of 12.1 rpm.

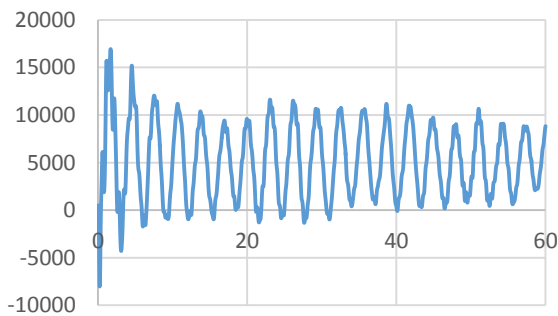


**Figure 12.** Side-wise bending moment (kN.m) of NREL 5MW tower time history at normal operation, wind velocity of 11.4 mps and rotor speed of 12.1 rpm.

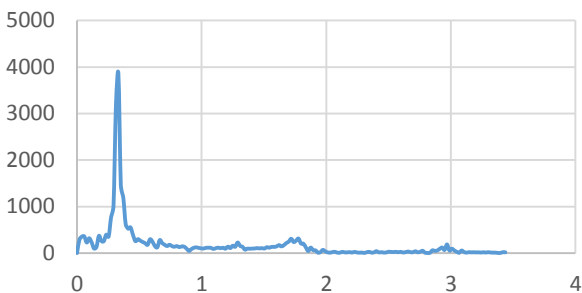


**Figure 13.** Frequency (Hz) spectrum of for-aft bending moment of NREL 5MW tower at normal operation, wind velocity of 11.4 mps and rotor speed of 12.1 rpm.

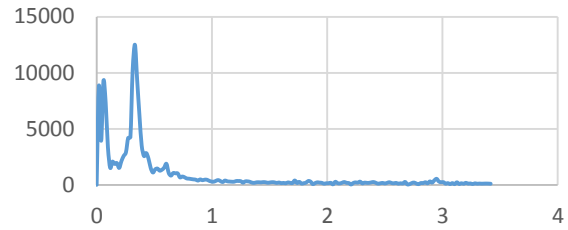


**Figure 14.** Frequency (Hz) spectrum of side-wise bending moment of NREL 5MW tower at normal operation, wind velocity of 11.4 mps and rotor speed of 12.1 rpm.

The previously depicted dominant frequencies of wind turbine sections are summarized in table 7. The results of this work are compared with those obtained in 0 via the FAST simulation software, which reveals a good agreement.

**Table 7.** Comparison between the results of this work and those obtained in 0

| Mode                | Natural frequency (Hz) |              |
|---------------------|------------------------|--------------|
|                     | Ref. [17]              | Present work |
| 1st tower bending   | 0.324                  | 0.33         |
| 1st rotor edge-wise | 1.0898                 | 1.09         |
| 2nd tower bending   | 2.9361                 | 2.97         |

### 4.3. Wind turbine parked condition

In this section, the wind turbine simulation is performed during the parked condition. It means that rotor is fixed, and all blades are pitched 90 degrees in downwind direction, wind speed is assumed to be 11.4 mps. Figure 15 and figure 16 show the blades root bending moment at edge-wise and flap-wise directions, respectively.

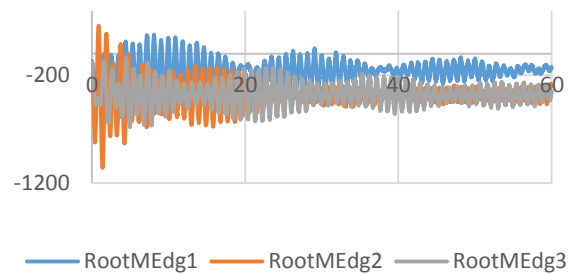


**Figure 15.** Root edge-wise bending moment (kN.m) of NREL 5MW blades time history at parked condition, wind velocity of 11.4 mps and fixed rotor.

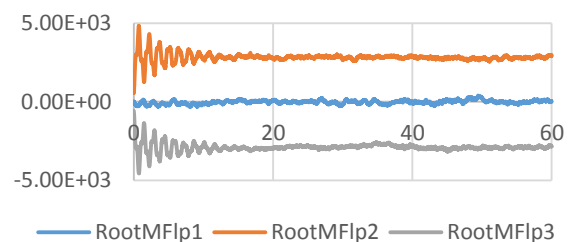


**Figure 16.** Root flap-wise bending moment (kN.m) of NREL 5MW blades time history at parked condition, wind velocity of 11.4 mps and fixed rotor.

Since the blade is pitched 90 degrees, figure 15 shows the out of plane bending of the blades, while figure 16 shows the in plane bending of blades. Hence, figure 16 represent the rotor deformation mode of figure 7. Rotor deformation mode corresponding to figure 15 is represented in figure 17. The frequency spectra of figure 15 and figure 16 are represented in figure 18 and figure 19.



Figure 17. Schematic description of asymmetric out of plane bending mode of rotor 0.

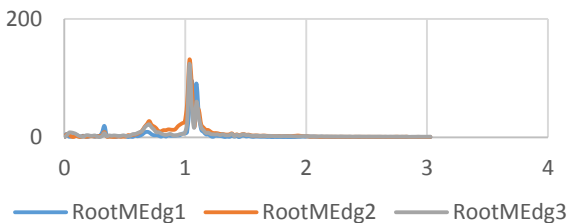


Figure 18. Frequency (Hz) spectrum of root edge-wise bending moment of NREL 5MW blades at parked condition, wind velocity of 11.4 mps and fixed rotor.

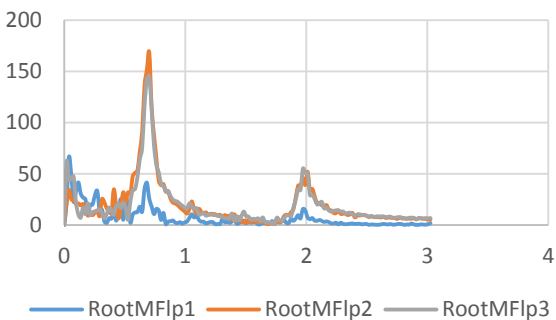


Figure 19. Frequency (Hz) spectrum of root flap-wise bending moment of NREL 5MW blades at parked condition, wind velocity of 11.4 mps and fixed rotor.

The dominant peak in figure 18 corresponds to the first edge-wise bending mode of blade with the frequency of 1.03 Hz. Figure 19 has two dominant peaks at 0.7 Hz and 1.97 Hz, which correspond to the first and second flap-wise bending modes of the blade.

Figure 20 and figure 21 show the for-aft and side-wise bending modes of the tower in the parked condition of the turbine.

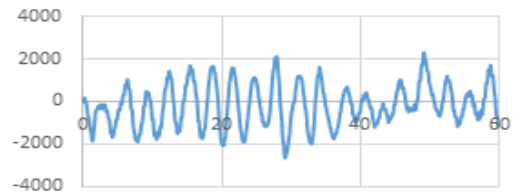


Figure 20. For-aft bending moment (kN.m) of NREL 5MW tower time history at parked condition, wind velocity of 11.4 mps and fixed rotor.

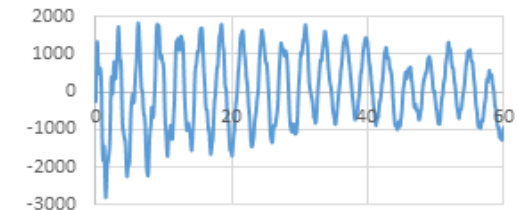


Figure 21. Side-wise bending moment (kN.m) of NREL 5MW tower time history at parked condition, wind velocity of 11.4 mps, and fixed rotor.

The frequency spectra of these tower bending modes is presented in figure 22 and figure 23. The dominant peak in figure 22 occurs at 0.3125 Hz, which is equal to the first fore-aft vibration mode of the tower. Also the second fore-aft vibration mode at 3.02 Hz has obvious effects.

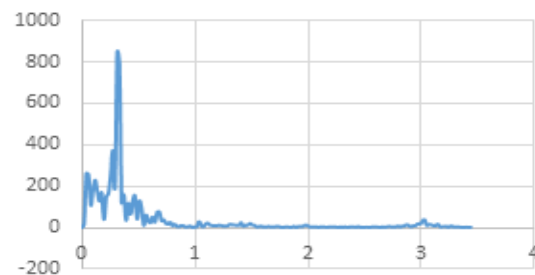


Figure 22. Frequency (Hz) spectrum of for-aft bending moment of NREL 5MW tower parked condition, wind velocity of 11.4 mps and fixed rotor.

In figure 23, the dominant peak corresponds to 0.332 Hz, which is the first side-wise bending vibration mode. Also the second corresponding vibration mode appears at 2.85 Hz.

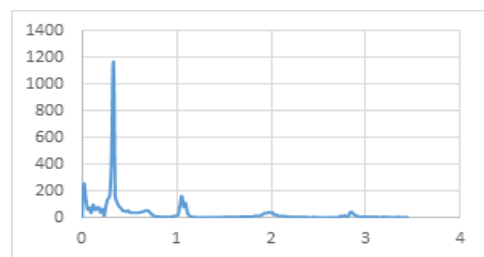


Figure 23. Frequency (Hz) spectrum of side-wise bending moment of NREL 5MW tower parked condition, wind velocity of 11.4 mps and fixed rotor.

Figure 22 has a peak at 0.68 Hz, which corresponds to the first blade flap-wise bending mode. Hence, contribution of the first flap-wise bending vibration mode of blade in fore-aft vibration of blade is obvious. This effect occurs in the parked condition, and does not appear in the wind turbine normal operation. It should be noted that contribution of the first edge-wise bending and second flap-wise bending of blade in fore and aft bending of tower is rather small. On the other hand, the contribution of the first edge-wise bending mode at the frequency of 1.05 Hz in the side-wise bending of tower is obvious. Hence, it could be concluded that the flap-wise bending modes of blade have minor effects on the tower vibrations in wind turbine normal operation but their effects become dominant during the parked conditions. Contrary to this phenomenon, the edge-wise bending vibration modes of blade has major effects on the tower vibrations during wind turbine normal operation, which become less important during the wind turbine parked conditions.

## 5. Conclusion

The modal dynamics of NREL 5 MW demonstration wind turbine was investigated in this work. In this regard, the FAST design tool was implemented, which simulated a complete wind turbine operation. The wind turbine was analyzed in two points of operations: normal operation with rated wind speed and rated rotor speed, parked condition with rated wind speed and fixed rotor. The modal dynamics of blade, tower, and whole wind turbine was investigated, and the corresponding natural frequencies and mode shapes were outlined. Afterwards, the blade root and tower root bending moments were analyzed for wind turbine at operation. The contribution of each vibration modes in the aforementioned bending moments was investigated in detail. It was shown that the tower vibration during normal operation was highly influenced from the blade edge-wise bending mode. On the other hand, during the parked condition, the effects of flap-wise bending modes became more dominant. The stiffening effect of the rotor speed on the first and second blade's vibration modes was outlined.

## 6. References

[1] Alayi, R., Jahangiri, M., Guerrero, J. W. G., Akhmadeev, R., Shichiyakh, R. A., and Zanghaneh, S. A. (2021). Modelling and reviewing the reliability and multi-objective optimization of wind-turbine system and

photovoltaic panel with intelligent algorithms. *Clean Energy*, 5(4), 713-730.

[2] Alayi, R. and Velayti, J. (2021). Modeling/optimization and effect of environmental variables on energy production based on PV/Wind turbine hybrid system. *Jurnal Ilmiah Teknik Elektro Komputer dan Informatika (JITEKI)*, 7(1), 101-107.

[3] Alayi, R., Zishan, F., Seyednouri, S. R., Kumar, R., Ahmadi, M. H., and Sharifpur, M. (2021). Optimal load frequency control of island micro-grids via a PID controller in the presence of wind turbine and PV. *Sustainability*, 13(19), 10728.

[4] Ganjei, N., Zishan, F., Alayi, R., Samadi, H., Jahangiri, M., Kumar, R., and Mohammadian, A. (2022). Designing and Sensitivity Analysis of an Off-Grid Hybrid Wind-Solar Power Plant with Diesel Generator and Battery Back-up for the Rural Area in Iran. *Journal of Engineering*, 2022.

[5] The world wind energy association website (2022), Available:

<https://wwindea.org/worldwide-wind-capacity-reaches-744-gigawatts/>.

[6] The national renewable energy website (2022), Available:

<https://www.nrel.gov/wind/nwtc/fast.html>

[7] Heinz, J. C. et al. (2016). Vortex-induced vibrations on a modern wind turbine blade, *Wind Energy*, Vol. 19, pp. 2041–2051.

[8] Bak, C., et al. (2013). The DTU 10-MW reference wind turbine in Danish Wind Power Research (Danish Technical University).

[9] Skrzypiąski, W. et al. (2014). Vortex-induced vibrations of a DU96-W-180 airfoil at 90 angle of attack, *Wind Energy*, Vol. 17, pp. 1495–1514.

[10] Lekou, D. et al. (2015). AVATAR deliverable D1.2: Reference blade design, Technical Report No. D1.2 (ECN Wind Energy, Petten, The Netherlands).

[11] Horcas, S. G. et al. (2020). Vortex induced vibrations of wind turbine blades: Influence of the tip geometry, *Physics of Fluids*, Vvol. 32, 065104.

[12] Bortolotti, P., et. al. (2019). Systems engineering in wind energy—WP2.1 reference wind turbines, Report No. NREL/TP-5000-73492.

[13] Hoang, M. C. et al. (2015). Experimental study on aerodynamic coefficients of yawed cylinders, *Journal of Fluids and Structures*, Vol. 54, pp. 597–611.

- [14] Bourguet, R. and Triantafyllou, M. S. (2015). Vortex-induced vibrations of a flexible cylinder at large inclination angle, *Philosophical Transactions of the Royal Society A*, Vol. 373, 20140108.
- [15] Horcas, S. G. et al. (2019). Suppressing vortex induced vibrations of wind turbine blades with flaps, In: Ferrer, E. and Montlaur, A. (Eds.), *Springer Tracts in Mechanical Engineering*, pp. 11–24.
- [16] Jonkman, B. and Jonkman, J. (2016). *Fast V8. 16.00 a-bjj*. NREL.
- [17] Jonkman, J. et al. (2009). *Definition of a 5-MW reference wind turbine for offshore system development*, NREL.
- [18] Farsadi, T. and Kayran, A. (2021). Flutter study of flapwise bend-twist coupled composite wind turbine blades, *Wind and Structures*, Vol. 32 (3), pp. 267-281.
- [19] Hansen, M. (2007). Aeroelastic instability problems for wind turbines, *Wind Energy*, Vol. 10(6), pp. 551–577.
- [20] Becker, M. (2017). *Fastfoam-an aero-servo-elastic wind turbine simulation method based on CFD*.
- [21] Mettam, G.R. and Adams, L. B. (1999). How to prepare an electronic version of your article, In: Jones, B.S. and Smith, R.Z. (Eds.), *Introduction to the Electronic Age*. E-Publishing Inc., New York, pp. 281-304.